Tailoring morphology and mechanical properties of PLA/PBSA blends optimizing the twin-screw extrusion processing parameters aided by a 1D simulation software

Vito Gigante [a,b,*,1], Laura Aliotta [a,b,1], Bianca Dal Pont [a], Vincenzo Titone [b,c], Luigi Botta [b,c], Francesco Paolo La Mantia [b,c], Andrea Lazzeri [a,b]

[a] *Department of Civil and Industrial Engineering, University of Pisa, L.go L. Lazzarino 1, 56122, Pisa, Italy*
[b] *Interuniversity National Consortium of Materials Science and Technology (INSTM), Via Giusti 9, 50121, Firenze, Italy*
[c] *Department of Engineering University of Palermo, Viale Delle Scienze, 90128, Palermo, Italy*

ARTICLE INFO	ABSTRACT
	To promote sustainability, the adoption of biobased and biodegradable plastics is a compelling solution. However, the successful utilization of these materials is contingent upon achieving desired properties and the ability to scale up production processes. Particularly in the case of blend systems, synergising the advantages of different polymers is essential. Moreover, assessing processing behavior and optimizing parameters are pivotal. This study aims to improve the extrusion process parameters selection using a 1D software-assisted Design of Experiments (DoE) approach. Polylactic acid (PLA) and polybutylene succinate-co-adipate (PBSA), varying PLA/PBSA ratios, were analysed simplifying and expediting the parameters selection. Remarkably, even in the absence of compatibility agents, this work demonstrates the potential to modify the structure, thereby influencing properties and performance by manipulating the process conditions.

1. Introduction

In recent years, it is a well-known fact that the growing environmental impact of plastics has become increasingly evident and concerning [1]. Despite this widespread awareness, the unique properties and ease of processing polymers have led to a significant increase in global plastic production (approximately 270 million tonnes in 2010, estimated to be around 390 million tonnes in 2021 [2]). As a result, managing plastic waste has become an ongoing challenge, with an estimated 8 million tonnes of plastic ending up in the oceans annually [3]. Moreover, the detrimental effects of plastics extend beyond marine ecosystems, as they can pollute soils, impact vegetation, and damage natural habitats [4]. To address these issues, many countries have implemented bans or restrictions on single-use plastic bags and non-recyclable plastic products, emphasizing the urgent need to adopt sustainable solutions that reduce the reliance on virgin plastic [5]. Developing bio-based, biodegradable, or compostable alternatives represents a crucial pathway towards achieving this goal, particularly to reduce dependence on oil resources [6]. In fact, bioplastics are becoming a viable alternative to traditional plastics and

their uses; currently their account is just 1 % of the total world plastic generated, however, through 2025, yearly growth rates are expected to be about 30 % [7]. Utilizing bio-based and biodegradable plastics for specific applications presents a promising solution, considering the need to emancipate from fossil fuel-based resources [8], but the full utilization of bioplastics depends on achieving desired final properties and the ability to scale up production processes, also adapting the current plants and manufacturing techniques [9].

One potential solution that has received considerable attention in recent years is the use of polylactic acid (PLA), a biobased semicrystalline aliphatic polymer, derived from sugarcane corn starch and cassava roots and belonging to the polyester family [10], that occupies a key position in the bioplastic market with an annual industrial production of approximately 400,000 tonnes [11]. Nevertheless, challenges need to be overcome for specific applications of PLA, such as enhancing its ductility, impact resistance and thermal stability to be processed for packaging or agricultural items [12].

On an industrial scale, physical polymer blending represents the simplest and most cost-effective solution, as it allows the combination of

---

Table 1
Blends name and composition.

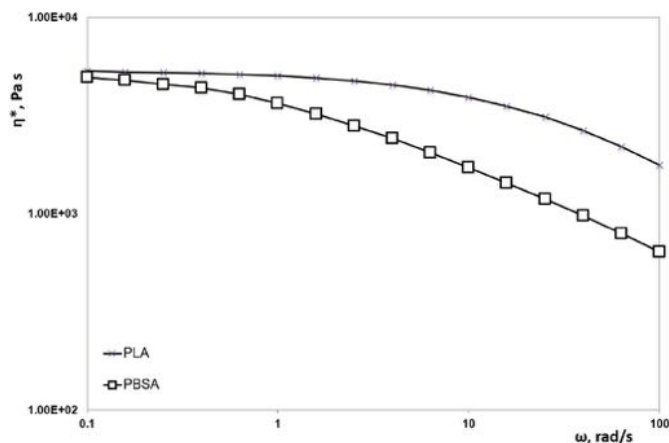| Formulation name	PLA (wt.%)	PBSA (wt.%)
PLA95PBSA5	95	5
PLA85PBSA15	85	15
PLA75PBSA25	75	25

two polymers in a physical manner to compensate for the individual disadvantages of each component. This simple approach of physical blending with a more ductile polymer has been used in many attempts also for PLA [13–17] and, among the various investigated biodegradable

Fig. 1. Flow curves at 190 °C of pure PLA and pure PBSA.

Table 2
Set of data entered in Ludovic Software for pure polymers.

PLA LX175		
Thermal properties	Melting temperature (°C)	168
	Melting enthalpy (kJ/kg)	40.32
	Solid phase	
	Heat capacity (J/kg/°C)	1314
	Density (kg/m^3)	1240
	Thermal conductivity (W/m K)	0.111
	Liquid phase	
	Heat capacity (J/kg/°C)	2140
	Density (kg/m^3)	1098
	Thermal conductivity (W/m K)	0.195
Rheological parameters	Power Law Index	0.436
	Carreau-Yasuda Index	0.679
PBSA FD92PM		
Thermal properties	Melting temperature (°C)	88
	Melting enthalpy (kJ/kg)	142.25
	Solid phase	
	Heat capacity (J/kg/°C)	1300
	Density (kg/m^3)	1240
	Thermal conductivity (W/m K)	0.190
	Liquid phase	
	Heat capacity (J/kg/°C)	2100
	Density (kg/m^3)	1100
	Thermal conductivity (W/m K)	0.220
Rheological parameters	Power Law Index	0.243
	Carreau-Yasuda Index	0.320

polymers, poly(butylene succinate-co-adipate) (PBSA) exhibits superior eco-efficiency compared to other biopolymers and boasts a high production capacity of approximately 100,000 tons per year highlighting the possibility, also in scale-up, of modulating PLA brittleness by blending it with PBSA [18,19]. Apart from the blend composition, the morphology of polymer blends is influenced by various processing parameters. In recent years, researchers from numerous groups have extensively explored the impact of process parameters on the morphology evolution of polymer blends, especially considering that twin-screw extruders are widely utilized for industrial-scale preparation of these blends [20–22]. Indeed, in order to develop interesting blends in terms of technology and application there is a need to optimize process parameters to at least a semi-industrial level to tailor the properties of the final blend [23]. Industrial-scale polymer blending is typically conducted in twin-screw extruders [24]; although the correlation between processing, morphology, and properties is well known, the identification of optimal processing conditions, including screw speed, feeding rate, and shear rate, is still approached through trial and error [25]. Indeed, it is crucial to have control over the blend morphology since it profoundly affects the material properties [26]. The evolution of the morphology in a biphasic system is influenced by the blend composition, processing conditions, rheological properties, and interfacial tension of the two constituents [27]. To simplify and speed up this selection process, software tools have been developed to provide insights into the evolution of various quantities (e.g., temperature, viscosity, shear rate, filling ratio) along the screw axis based on geometric, thermal, rheological, and process inputs [28]. These tools enable predictions of the most suitable operating conditions for achieving desired material properties aided also by tailored design of experiments [29].

Therefore, the objective of this study is to optimize the extrusion process parameters through a 1D software-aided Design of Experiments (DoE) approach with Ludovic® Software, simplifying and expediting the parameter selection process for blends of polylactic acid (PLA) and polybutylene succinate-co-adipate (PBSA) with varying PLA/PBSA ratios.

Ludovic® software, indeed, has been developed to provide data on the evolution of many outputs (temperature, viscosity, shear rate) along the screw axis [30]. The impact of processing parameters, particularly the influence of screw profile, on the microstructure and properties of biopolymeric blends remains poorly investigated. To fully utilize these blends in industrial applications, it is crucial to systematically study their processing behavior and optimize the processing conditions.
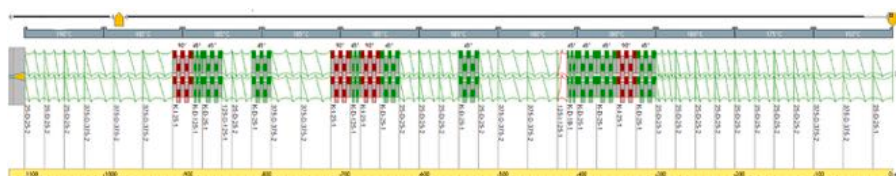
For all these reasons, in the present work, the simulation results have been compared with real extrusions in a constrained range of process conditions; in addition morphological, rheological, mechanical and DMTA tests have been performed directly on the filaments produced avoiding a secondary process that could influence the final properties. The materials compounded, employing the best processing parameters, showed a satisfying accordance with the predictions, demonstrating the usefulness of the simulation tool.

Fig. 2. Geometrical design of Pisa University Twin-screw Extruder.

Table 3
Filament produced by twin-screw extrusion.

	RPM		
pbsa content (wt.%)		300	350	400
	5			
	15			
	25			

2. Materials and methods

2.1. Materials

- Poly(lactic) acid (PLA) with trade name Luminy LX175 was purchased by Total Corbion PLA. It is an extrusion PLA grade that contains about 4 % of D-lactic acid units. [density: 1.24 g/cm^3; melt flow index (MFI) (210 °C/2.16 kg): 6 g/10 min].
- Poly(butylene succinate-co-adipate) (PBSA) with trade name BioPBS FD92PM was purchased from Mitsubishi Chemical Corporation. It is a ductile semicrystalline copolymer of succinic acid, adipic acid and butandiol. [density of 1.24 g/cm^3; MFI (190 °C, 2.16 kg): 4 g/10 min].

Polylactic acid (PLA)/polybutylene succinate-co-adipate (PBSA) blends with the ratios showed in Table 1 have been selected and produced in such a way PBSA can be considered as a dispersed phase (no co-continuity as demonstrated by Aliotta et al. [18]) and the total biobased content is at least 90 %.

2.2. Setting of simulations parameters

DoE analysis and twin screw simulations have been conducted with Ludovic (SC-Consultants, Saint Etienne, France) aiming to deliver a comprehensive thermo-mechanical analysis of compounding within a twin-screw extruder. The outcome of these analyses is a 1-D description of the material behavior along the screw and inside the die, considering stationary conditions [31]. In preparation for launching the simulation in the software, a comprehensive characterization of the pure polymers is necessary in order to gather all the required information. Melting temperatures and melting enthalpies were obtained from DSC analysis (Q200 TA instruments, Newcastle, UK) in first run with a heating at 10 °C/min from 0 to 200 °C, while to assess the preliminary rheological behavior of the materials viscosity Carreau-Yasuda analytical model Arrhenius-modified (Equation (1)) has been applied using parameters extrapolated from experimental data (as example in Fig. 1 the flow curves at 190 °C of pure PLA and pure PBSA have been reported).

$$\eta = \frac{\tau_y}{\dot{\gamma}} + \eta(T)(1 + (\lambda(T)\dot{\gamma})^a)^{\frac{m-1}{a}}$$ (1)

Where $\eta(T)$ and $\lambda(T)$ follow a thermo-dependency of the Arrhenius type, m is the power-law index, a is the Carreau-Yasuda index, τ_y is the shear stress, $\dot{\gamma}$ is the shear rate and η the viscosity.

The complete set of data entered in Ludovic Software is shown in Table 2.

In order to understand the thermal and rheological changes associated to the resulting morphology, occurring during the extrusion process, the first step entails designing the screw profile geometrically. Indeed, giving 3 input types (product, geometry and process) Ludovic returns a 1-D description under stationary conditions of the material behaviour along the screw and inside the die. A COMAC twin-screw extruder (Milan, Italy) located at the UNIPI laboratories, featuring specific dimensions of L/D = 44, diameter = 25 mm, and centreline = 21 mm has been used and, therefore, geometrically designed in the software. This extruder comprises 11 barrels, with venting facilitated in zone 10 and feeding in zone 1. In each simulation, a 1 % loss of oligomers and vapor from venting was considered in zone 10. The screw design, as illustrated in Fig. 2, consists of distinct sections: the initial part encompasses conveying elements with gradually decreasing pitch to transport the solid material to the melting zone (zone 4), where kneading elements with diverse orientations promote the melting process.

Subsequently, a series of alternating mixing elements and conveying elements are incorporated to ensure both distributive and dispersive mixing throughout the extrusion process, leading up to the outlet. At the outlet, two transport elements with narrower pitch are employed to increase the outlet pressure. Ultimately, the die configuration involves a first '8-shape' nozzle that accommodates the screw tips and conveys the molten blend into a circular nozzle, having a diameter of 2 mm. The temperature profile in the eleven barrels was set up following careful experience from previous works [32] as follows: 150-175-180-180-180-185-185-185-185-185-190. To simulate the effect of heat exchange of the die, cylinder and screw a value of 1000 W/m^2 K has been defined as recommended in literature [33]. Regarding flow rate and screw speed a Design of Experiments (DoE) has been
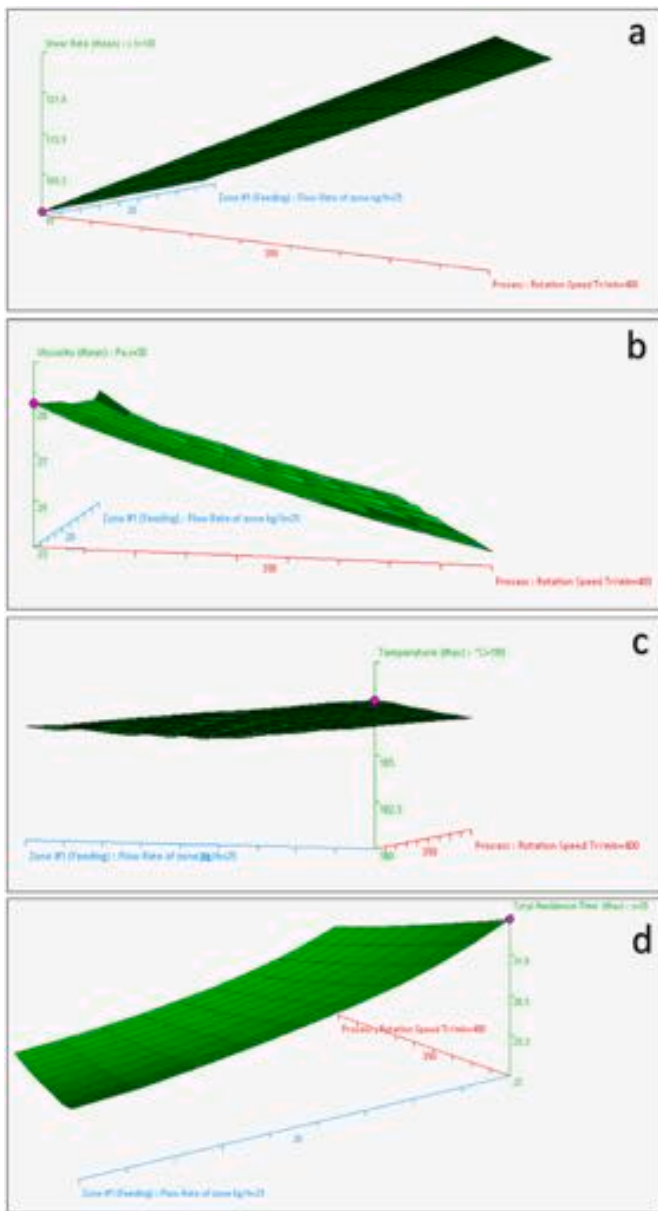
Fig. 3. PLA95PBSA5 behavior regarding: a) shear rate, b) viscosity, c) Maximum temperature d) residence time.

designed to find the best process conditions shifting flow rate from 15 to 25 kg/h and screw speed from 300 to 400 rpm with 10 intermediate steps.

2.3. Processing of the blends

Following DoE results, that will be discussed in detail in the next sections, "real" extrusion have been carried out to produce 9 typologies of filaments with a mean diameter of 1.2 mm (Table 3).

The three formulations were subjected to a drying process using a Piovan DP 604 dryer (Piovan S.p.A., Venice, Italy) before being processed in a semi-industrial twin-screw extruder, the Comac EBC 25HT (Milan, Italy). Consistent with the simulator, a temperature profile was adopted, ranging from 150 °C to 190 °C with specific temperature settings as follows: 150/175/180/180/180/185/185/185/185/185/190 °C. Three different screw rotation speeds were chosen (300-350-400 rpm), while maintaining a constant total mass flow rate of 15 kg/h. This approach ensured that residence times, exit pressures, and
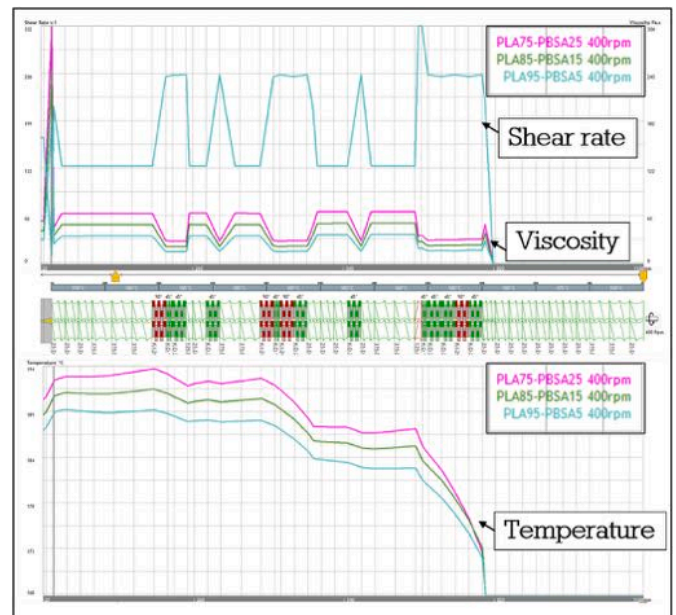

Fig. 4. Shear rate, temperature and viscosity behavior along the screws profile for the three formulations studied maintaining constant the screw speed (400 rpm).
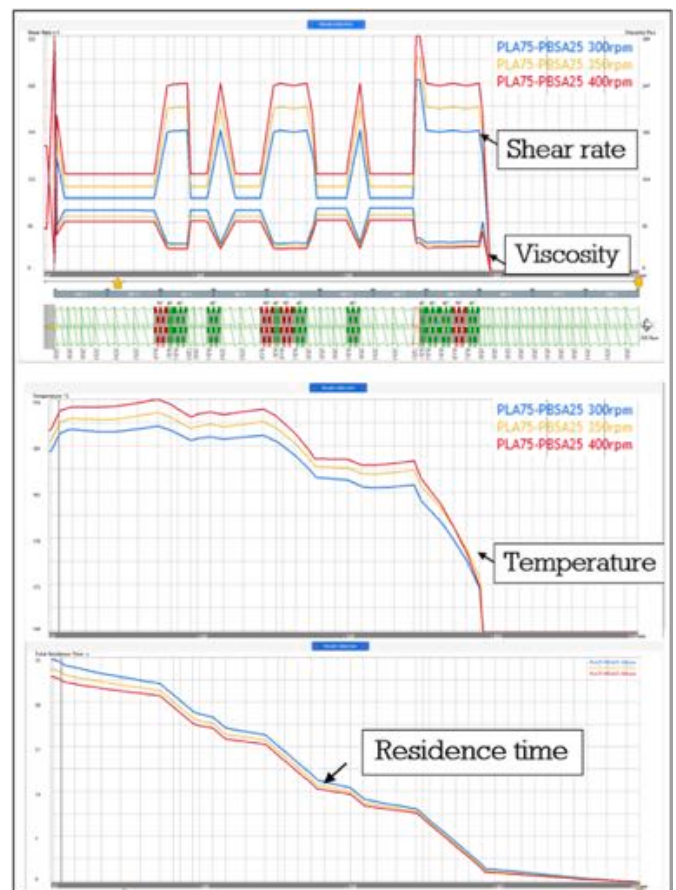

Fig. 5. - Shear rate, temperature, residence time and viscosity behavior along the screws profile varying screw speed but maintaining constant the PBSA content.

temperatures matched the software predictions.

2.4. Characterization methods

All the tests have been performed directly on the filaments produced avoiding a secondary process that could influence the final properties.

The morphology of the blends was examined using scanning electron microscopy (SEM; Quanta 200 ESEM, FEI, Hillsboro, OR, USA). To do this, the samples were broken under liquid nitrogen and attached to the sample holder to observe the fracture surface. To prevent electrostatic charging under the electron beam, all the samples were coated with a thin layer of gold for 120 s under an argon atmosphere using Scancoat Six Edwards (Crawley, UK). The dimensional distribution of the PBSA dispersed phase varying formulation and screw speed has been calculated from the SEM images obtained using the Image J® software (NIH, Bethesda, MD, USA). About 200 particles were examined for each typology.

Rheological tests of shear flow at low shear rates were performed using a rotational rheometer (ARES-G2, TA Instruments, Newcastle UK) in a plate-plate mode. Operatively, tests were conducted at 190 °C (the temperature at the exit of the nozzle) with an imposed strain of 5 % and sweeping frequency of 0.1–100 rad/s on the filament itself simply granulated and placed between the two plates. The tests were performed in triplicate.

Tensile tests were conducted on 10 filaments for each formulation using a MTS Criterion 43 (MTS Systems Corporation, Eden Prairie, MN, USA) and a 1 kN load cell, with a grip distance of 80 mm and a test speed of 10 mm/min. Although filaments provide a convenient means of measuring mechanical properties, a universally standardized testing technique for evaluating their tensile properties is currently lacking. In this study, we followed the procedure outlined by Rodrigues et al. [34] for conducting the tests.

The dynamic mechanical thermal analysis (DMTA) was performed on a on a Gabo Eplexor® 100 N (Gabo Qualimeter GmbH, Ahlden, Germany). Samples with a length of 40 mm were cut and placed on a tensile geometry configuration. The temperature used in the experiment ranged from −60 °C to 110 °C with a heating rate of 2 °C/min and a frequency of 1 Hz to evaluate, under oscillating loading are the storage modulus (E′) behaviour switching the temperature.

The mechanical results were subjected to statistical analysis, i.e., the mechanical properties of interest, meeting the criteria for statistical significance. In particular, the F-test (ANOVA) was applied and a p-value <0.05 was selected as statistically significant limit.

Thermal properties of PLA/PBSA filaments were investigated by calorimetric analysis (Q200 TA- DSC). Nitrogen, set at 50 mL/min, was used as purge gas for all measurements. To better understand if an eventual crystallization occurred due to the extrusion process, the thermal properties were evaluated considering only the first DSC heating run (without deleting the thermal history). The samples, with mass between 10 and 12 mg, were sealed inside aluminum pans before measurement. The samples were quickly cooled from room temperature to −60 °C and kept at this temperature for 1 min. Then the samples were heated at 10 °C/min up to 200 °C. Melting temperature (T_m) and cold crystallization temperature (T_{cc}) of PLA were recorded at the maximum of the melting peak and at the minimum of the cold crystallization peak,
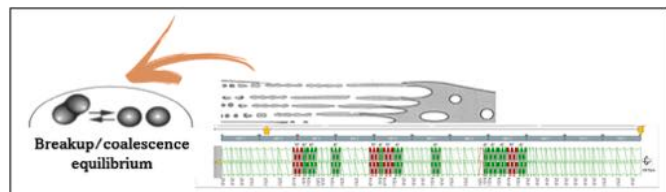
respectively. The enthalpies of melting and cold crystallization were determined from the corresponding peak areas in the thermograms. PLA crystallinity has been calculated according **Equation (2)**:

$$X_{cc} = \frac{\Delta H_{m,PLA} - \Delta H_{cc,PLA}}{\Delta H^0_{m,PLA} \bullet wt\%_{PLA}} \qquad (2)$$

where X_{cc}, is the crystallinity fraction of PLA ΔH_m and ΔH_{cc} are the melting and cold crystallization enthalpies respectively, while $\Delta H^0_{m,PLA}$ is the theoretical melting heat of 100 % crystalline PLA with a value of 93 J/g [35].

3. Results and discussion

3.1. Design of experiment: influence of feed rate and screw speed

A comprehensive 10-step Design of Experiments (DoE) was executed, manipulating feed rate and rpm, to scrutinize key processing properties (residence time, shear rate viscosity, and temperature, as depicted in Fig. 3) throughout the screw profile. It was ensured that all simulations converged, preventing potential motor overload due to excessive material or, conversely, material shortage [36]. The primary objective was to elucidate the intricate relationship between these process parameters and the final morphology of the three blends, establishing meaningful correlations with rheological and macroscopic properties.

Fig. 3 presents the characteristic response surfaces (green axis) obtained by varying feed rate and screw speed (blue axis, 15–25 kg/h - red axis, 300–400 rpm respectively) for the PLA95PBSA5 blend. Numerical values extrapolated to 9 couplings, considering extremes and an average matrix value, are provided in **Appendix A** for all formulations.

Simulation results indicate marginal differences in maximum temperature and average viscosity, while substantial variations in residence time and shear rate with simultaneous variations in flow rate and screw speed have been emerged. Flow rate principally influences residence time, higher flow rate results in shorter residence time. On the other hand, the shear rate is unaffected by the flow rate but highly influenced by the screw speed as confirmed by other research works in this field [37,38]. Since the main objective of this study is to examine how
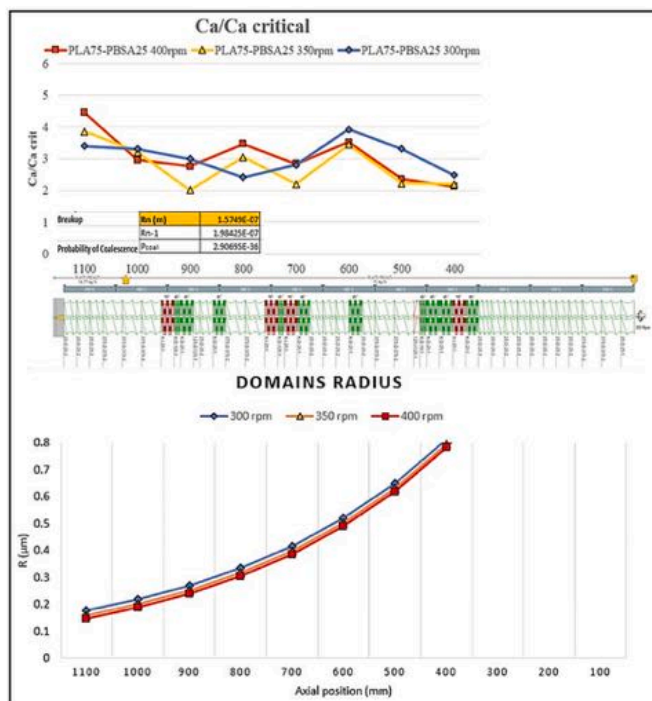

Fig. 6. Breakup/coalescence equilibrium for immiscible polymer blends along twin-screw extruder.

Fig. 7. Vergnes model application along the screw profile.
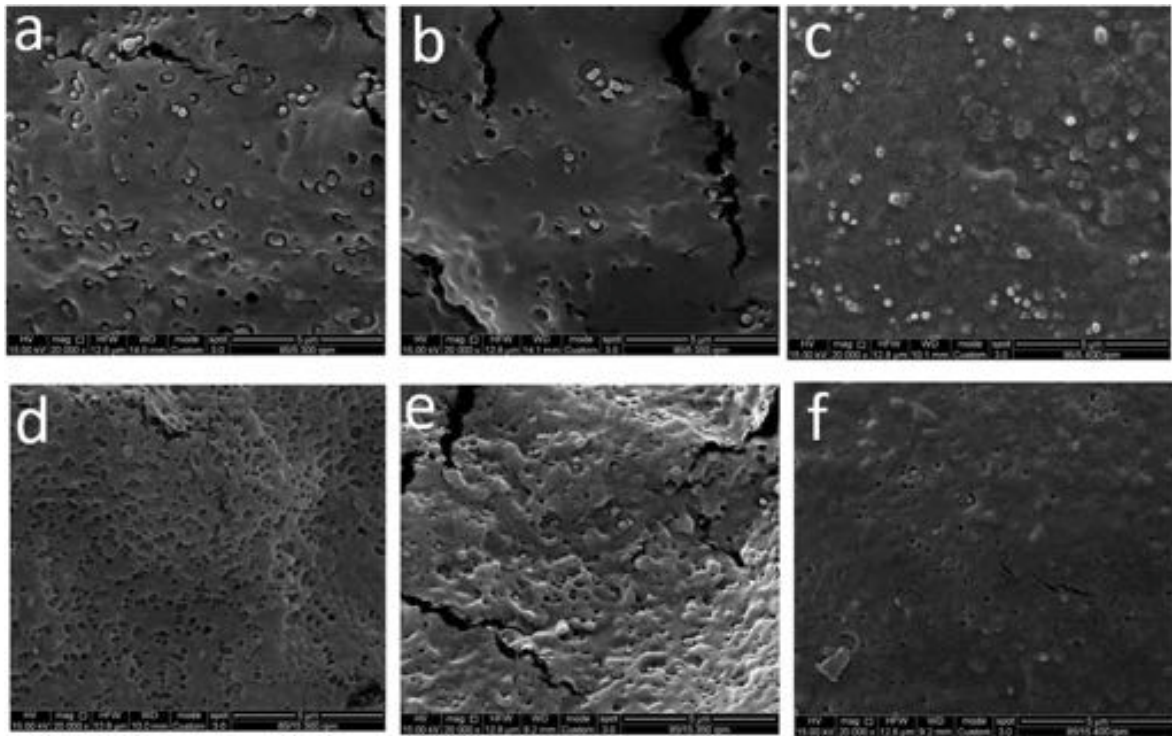
Fig. 8. Micrographs at 20000x for a) PLA95PBSA5 at 300 rpm, b) PLA95PBSA5 at 350 rpm, c) PLA95PBSA5 at 400 rpm, d) PLA85PBSA15 at 300 rpm, e) PLA85PBSA15 at 350 rpm, f) PLA85PBSA15 at 400 rpm.
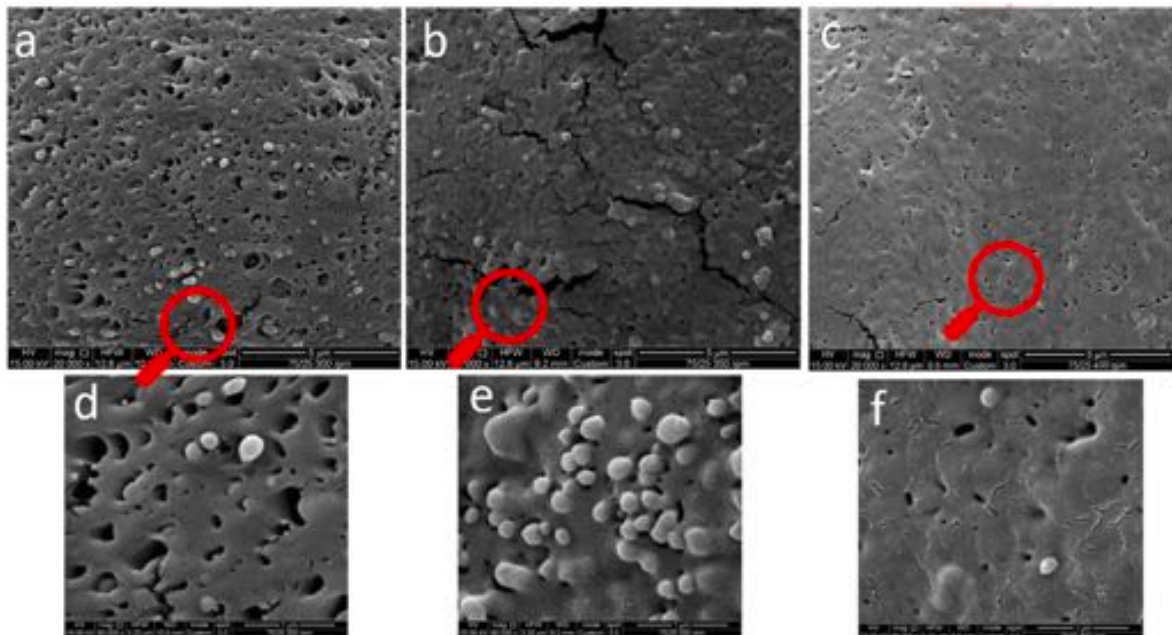
Fig. 9. Micrographs at 20000x for a) PLA75PBSA25 at 300 rpm, b) PLA75PBSA25 at 350 rpm, c) PLA75PBSA25 at 400 rpm, Micrographs at 80000x for PLA75PBSA25 at d) 300 rpm, e) 350 rpm, f) 400 rpm.

different morphologies influence the properties of the blends, it was decided, for the actual extrusions, to vary the screw speed to observe the effect on the shear rate, while keeping the flow rate constant at 15 kg/h.

This approach ensures an approximate 30 s residence time for all formulations, favouring distributive and dispersive mixing between PBSA and PLA phases without reaching degradation temperatures.

Going into further detail, Fig. 4 illustrates the differences in behavior at constant screw speed, while Fig. 5 shows the differences at constant

formulation. Indeed these are two interesting comparisons can be made by exploring the behavior of the properties along the previously designed screw profile, varying either the PBSA content or the screw speed. The analysis starts from the fourth barrel because it is considered the moment in which the polymeric material from pellet is then totally melted. The properties are depicted as a function of the axial distance along the screw.

Comparing the simulations at 400 rpm, the restricting elements
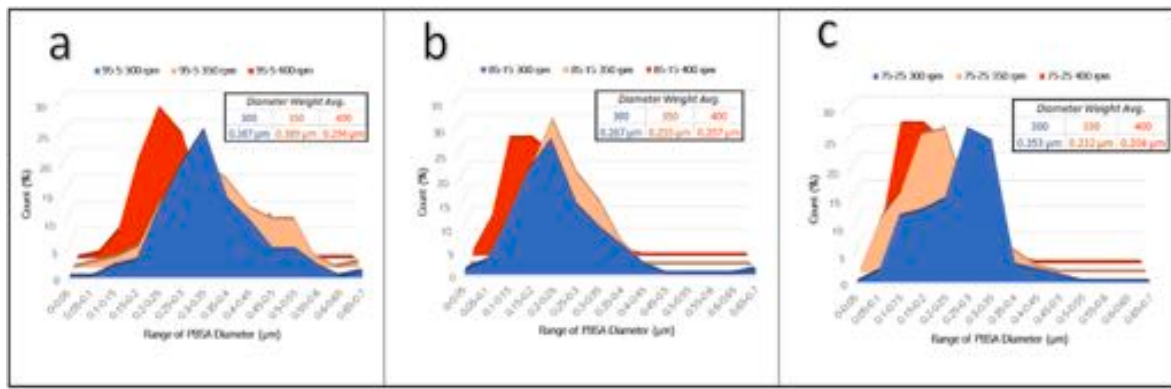
Fig. 10. Diameter distribution, varying screw speed, for a) PLA95PBSA5, b) PLA85PBSA15, c) PLA75PBSA25.

exhibit the highest shear rate values, which remain consistent for all the blends, while the conveying elements show lower $\dot{\gamma}$ values. This is in line with our expectations.

As it could be expected, comparing simulations at 400 rpm, the constraining elements consistently demonstrate the highest shear rate values across all blends, while the conveying elements exhibit lower shear rate values. Nevertheless, the shear rate variation observed can be described to the different staggering angles of the kneading elements. Notably, in the first kneading element, a substantial increase in temperature is observed, resulting from the significant increase in shear rate caused by these elements. Additionally, an increase in the quantity of

PBSA leads to higher total blend viscosity. As expected, no changes in residence times were recorded when varying the PBSA content.

Regarding Fig. 5, it is evident that the residence time is distributed along the screw elements, with approximately 2 s in each kneading element and 0.2 s in each conveying element.

As anticipated, a higher shear rate corresponds to increased energy dissipation, resulting in elevated temperatures. Consequently, it is expected that such temperature and shear rate increments will lead to a decrease in viscosity.

Fig. 11. Flow curves achieved at plate/plate rheometer for a) the 3 blends at 300 rpm b) the 3 blends at 350 rpm c) the 3 blends at 400 rpm d) PLA95PBSA5 varying screw speed, e) PLA85PBSA15 varying screw speed f) PLA75PBSA25 varying screw speed.

3.2. Vergnes model and simulation comparisons varying screw speed

Based on the data obtained from simulations, the next step was to attempt to predict the type of morphology and, if the existe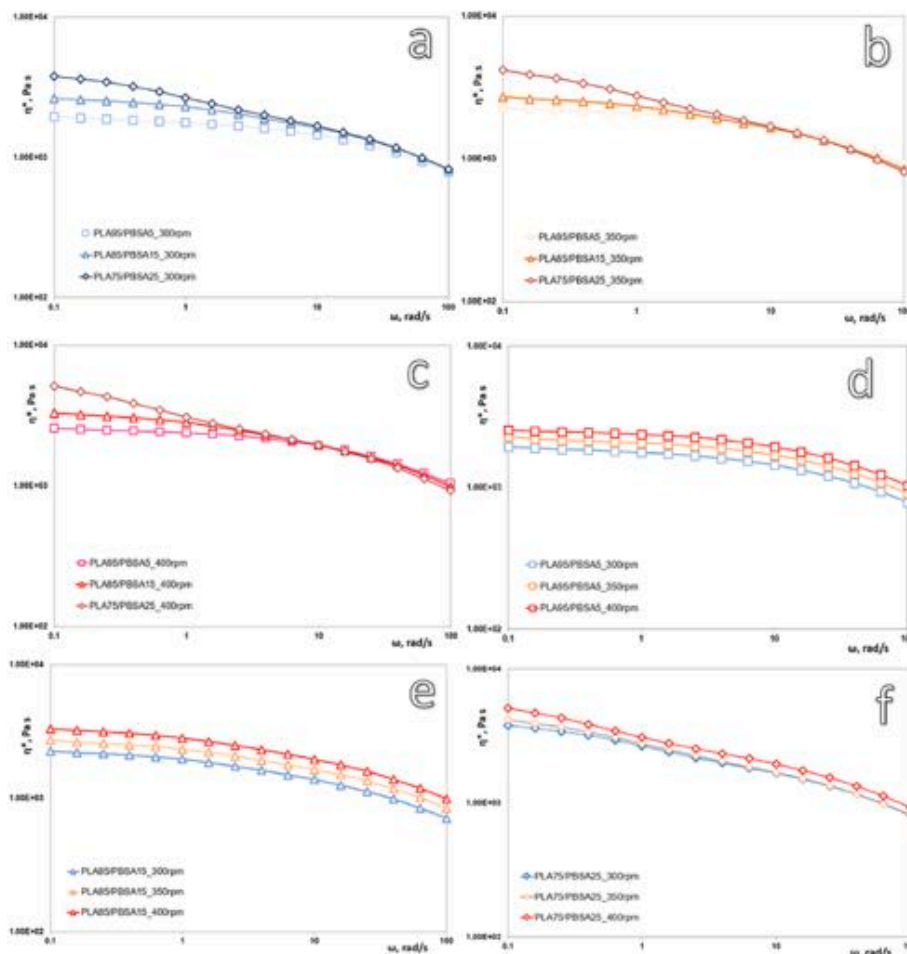nce of a dispersed phase in droplets within a continuous matrix was confirmed, also predict the particle sizes. The two primary mechanisms that drive changes in the immiscible polymer blend's morphology are *Breakup*, which reduces the size of the dispersed phase, and *Coalescence*, which has the opposite effect [39]. These two phenomena are in equilibrium with each other within an extruder where the stress field is quite complex, to favor breakup compatibilizers and other additives can be added [40] but to tailor the morphology solely by acting on the process parameters, one needs to optimize it towards the desired goal. In the case of non-Newtonian fluids, the droplets elongate in a direction perpendicular to the flow. As a result, their extremities are located in zones with varying velocities, leading to breakup [41].

Utracki et al. observed that the ideal conditions for disrupting a single droplet in an extruder (to increase the shear rate and decrease the viscosity of the dispersed phase) simultaneously promote coalescence [42]. To accurately describe the system's behavior, it is crucial to correctly choose the conditions for measuring viscosity along the screw profile [43] as illustrated in Fig. 6.

Furthermore, due to the presence of non-Newtonian fluids in the system, significant deviations can be observed, especially concerning viscosity ratios [44]. In this context Delamare & Vergnes provide a mathematical relationship that can provide insights into the final

dimensions of the dispersed phase after compounding. Specifically, they quantify the probability of coalescence and breakup occurring inside an extruder [45]. The analysis can only be referred to the case in which the concentration of the minor component is quite low because it would not be effective with co-continuous morphologies [46]. The model has been applied barrel by barrel to the blend formulations of the present work; briefly, the conditions for the breakup phenomenon to occur is expressed in Equation (3), otherwise the deformation of the dispersed fibrils occur but no breaking.

$$Ca > 2Ca_{critical} \qquad (3)$$

where:

$$Ca = \frac{\eta_{matrix}\dot{\gamma}R_{droplet}}{\Gamma_{12}} \qquad (4)$$

$$Ca_{critical} = \frac{\eta_{droplet}}{\eta_{matrix}} \qquad (5)$$

with $\dot{\gamma} = $ shear rate $\Gamma_{12} = $ interfacial tension $\eta = $ viscosity $R = $ *Dispersed Phase Radius*,

When the conditions for the breakup exist, that means that the ratio between capillary number and critical capillary number is major than 2, favourable conditions for the coalescence of droplets also occur in parallel, and the probability of coalescence is given by Equation (6):

$$P_{coal} = exp\left(\frac{-\pi}{8\dot{\gamma}\varphi t}\right) \bullet exp\left[-\frac{3}{2}\ln\left(\frac{R}{h^*}\right)Ca\right] \qquad (6)$$

with $\dot{\gamma} = $ shear rate $h^* = $ critical thickness $R = $ *Dispersed Phase Radius*

$\varphi = $ *volume fraction of dispersed phase* $t = $ *residence time*

At this point it is possible to predict the radius of the dispersed phase (Equation (7)) on the basis of volume conservation barrel by barrel (n); the result is then multiplied for the expression which considers the effect of coalescence:

$$R_n = R_{n-1}(2 - P_{coal})^{-\frac{1}{3}} \qquad (7)$$

Fig. 7 illustrates the outcomes of fitting the model to the blend with the highest PBSA content varying the screw speed. It is evident that the breakup condition is consistently maintained during the melting process along the extruder. Specifically, the ratio between the capillary number and the critical capillary number is predicted to be higher than 2, with elevated values corresponding to the melting and mixing elements. This correlation arises due to the higher shear rate, wherein drag forces predominate. The final iteration indicates an extremely low probability of coalescence (approximately 10^{-36}) across all screw speeds. As a result, it seems that a morphology characterized by a continuous phase and dispersed phase in droplets, with the absence of fibrils, can be predicted. Furthermore, the model forecast a trend of the particle radius of the dispersed phase that, based on the simulated barrel-by-barrel viscosity change, at the exit of the last barrel, could be approximately of 0.16 μm at 400 rpm by imposing a starting radius of 1 mm, as recommended in the literature for similar biopolymeric blends [47].

3.3. Morphological results and diameter distribution

To verify the accuracy of the predictive model, a morphological analysis of the strand exiting the nozzle was performed using SEM micrographs and subsequent size distribution measurements. From the comprehensive Fig. 8, in which PLA95PBSA5 and PLA85PBSA15 micrographs of the blends produced at 300, 350 and 400 rpm, it can be concluded that the morphology aligns with the expected breakup mechanism.

More specifically where PBSA particles appear as dispersed droplets within a continuous PLA matrix, and coalescence is practically absent
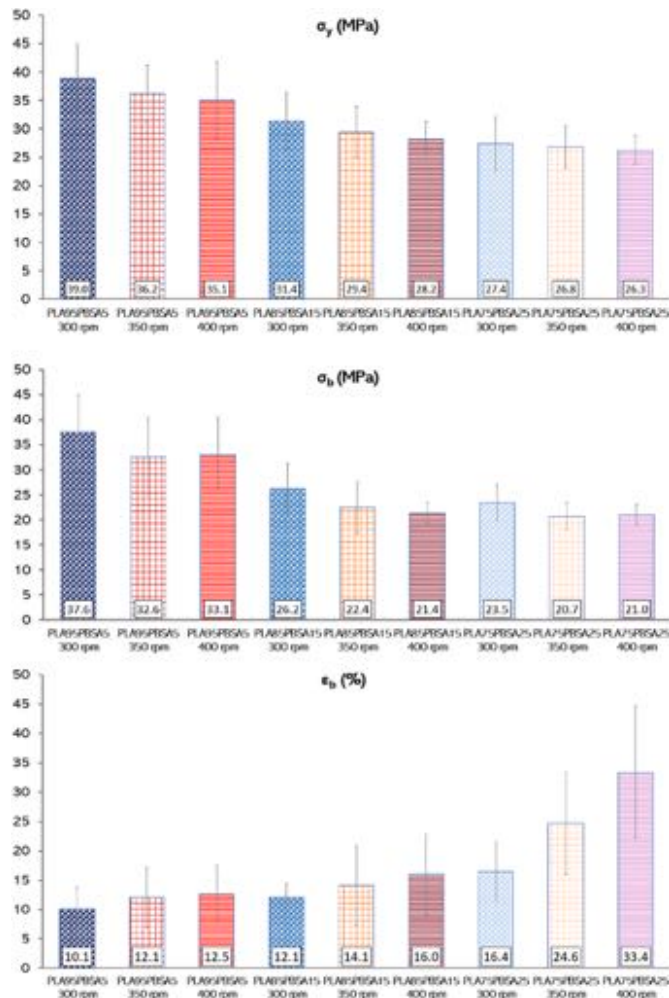

Fig. 12. Tensile properties for the filaments produced varying PBSA content and screw speed.

Table 4
- ANOVA statistical results.

Formulation name	Stress at yielding		Stress at break		Elongation at break	
	F-value	p-value	F-value	p-value	F-value	p-value
PLA95PBSA5	7.8877	0.0035	2.4493	0.1145	0.7838	0.4717
PLA85PBSA15	0.3098	0.7378	3.3724	0.0600	1.7109	0.2088
PLA75PBSA25	0.5626	0.5806	0.2680	0.7678	7.8609	0.0042
	The result is significant at p<0.05					
	The result is not significant at p<0.05					
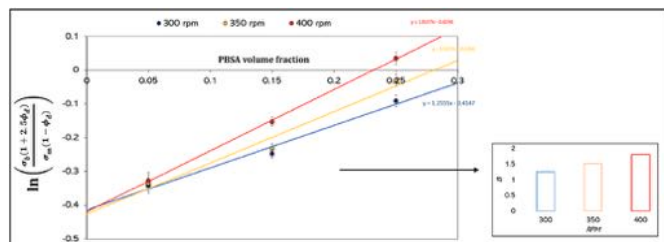
Fig. 13. Pukanszky model application.

for all formulations and screw speed tests. Of particular interest is Fig. 9 and the consequent diameter distribution (Fig. 10), which reveals a significant experimental difference for the PLA75PBAT25 blend, indeed in the latter case the effect of shear rate ensures a more pronounced breakup, resulting in a significantly smaller dispersed phase size, especially when the rubber component is more prevalent. According to the rubber toughening theories [48,49], this would guarantee enhanced ductility in the final material.

Moreover, always in Fig. 8, a zoom on the dispersed droplets has been evidenced (with micrographs carried out at 80000x) to evidence the morphologies differences of the filament fractur surfaces even if the blend formulation is the same: it is possible to state that processing conditions, and in particular the action of the shear rate inside the twin-screw extruder, modify the morphology of immiscible biopolymer blends made by PLA and PBSA. Definitely, for PLA75PBSA25 at 400 rpm average dispersed phase diameter (around 0.2 μm) has been found 24 % smaller with respect to 300 rpm.

It is crucial to comprehend now how this distinct morphology, induced by varying shear rates while maintaining the same formulation and residence time, impacts the rheological, mechanical and thermal properties of the blends.

3.4. Rheological results

The flow curves of all the blends measured with the rotational rheometer are shown in Fig. 11 and they have been carried out to understand whether structural differences may have arisen as a result of different PBSA concentration or, more importantly, as a result of the effect of different screw speed and processing conditions.

PLA95PBSA5 and PLA85PBSA15 exhibit a more marked Newtonian behavior at low shear rates, and by increasing the shear rate, the curves of the different formulations approach each other showing, then, no substantial differences in viscosity; this behavior has been evidenced also in a previous work for PLA-PBAT blends [50]. PLA75PBSA25, on the other hand, shows a decreasing trend in viscosity, thus more pseudoplastic, since very low values of shear rate; this behavior seems typical of PBSA and has also been found in the literature [51,52].

It is also attractive to discuss the results of the flow curves maintaining constant the PBSA content; it is evident that the experimental

points are equally spaced throughout the entire shear rate increment, but the highest viscosity values, at the same PBSA content, are observed for the blends extruded at 400 rpm. This is because the smaller size of the dispersed phase ensures a stronger melt strength, indeed the improved strength is a result of the reduced size of the dispersed phase and superior interaction as described by Anstey et al. for blends PP/PLA [53] or by Hale et al. [54] for PBT/ABS. Definitely, the droplet diameter decreases when screw speed and PBSA content increase, as described by Ding et al. [55]; therefore the interfacial area between PLA and PBSA increases and it can be considered another effect of the imposed difference in shear rate for compounding PLA/PBSA blends.

3.5. Tensile results

To assess the potential influence of different blends morphologies on their mechanical properties, tensile tests directly on the filaments were conducted. This approach ensured that the morphology remained unchanged avoiding subsequent processing, such as molding. In Fig. 12, the average results (along with relative deviations) of yield stress, stress at break, and elongation at break for the nine produced combinations were shown. The findings indicate that the variation in shear rate has only a minimal effect on mechanical strength and yielding point. As expected the fundamental parameter affecting these properties is the PBSA content in the blends. Additionally, the rubbery phase content significantly influences the ductility of the blends, leading to higher values of elongation at break. At this purpose it is important to focus the attention on the elongation at break data for the PLA75PBSA25, as it is intriguing to note that this particular combination highlights the most evident effect resulting from the application of a different screw speed.

At 400 rpm, thus with a higher imposed shear rate in the extruder, it was previously demonstrated that a morphology with smaller dispersed phase dimensions could be achieved, leading to increased melt strength.

Another evident outcome is the difference in ductility; therefore, it is possible to assert that the effect of the screw speed, ensuring better mixing, promotes an increase in ductility, but only when the PBSA content allows for such enhancement in this property. On the other hand, when the content of the rubbery dispersed phase is too limited, the action of the shear rate fails to increase ductility. However, this more impactful effect of the shear rate does not compromise the mechanical strength in the case of these biopolymeric blends since it remains almost unchanged as the screw speed varies. It is important to emphasize that ductility can be altered solely by manipulating an extrusion process parameter, while keeping the formulation constant; however to achieve even higher ductility, as demonstrated in previous studies, it is necessary to obtain a co-continuous morphology of PLA-PBSA by increasing the amount of PBSA in the blend [56–58].

To assess whether the mechanical property data have statistically significant relevance under identical formulations by varying screw speeds, an analysis of variance (ANOVA) was carried out and F value and p value are showed in Table 4. The outcome of this analysis indicates that the most statistically significant data point is the elongation at break
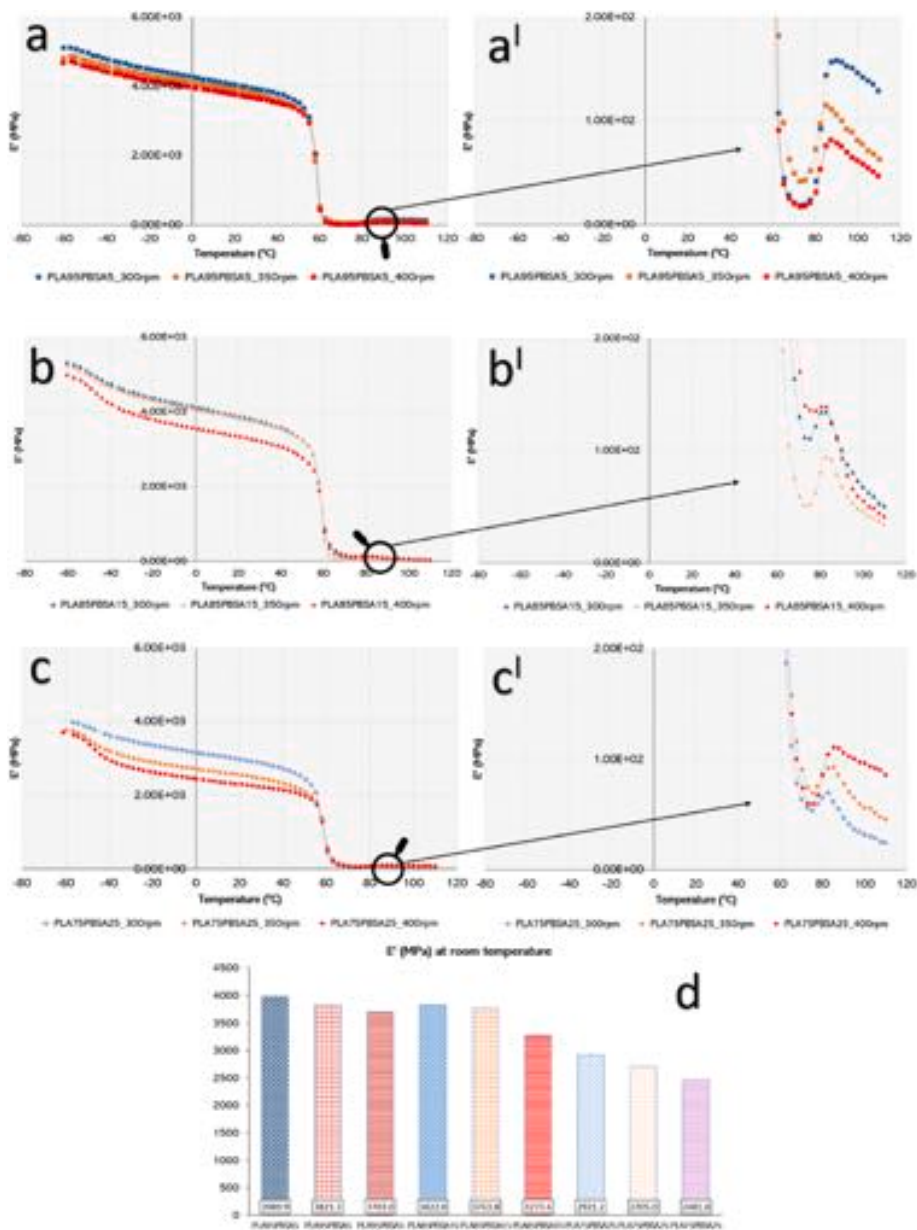
Fig. 14. Elastic response for a) PLA95PBSA5 varying the screw speed b) PLA85PBSA15 varying screw speed c) PLA75PBSA25 varying screw speed. a')b')c') represent the zoom of the data regarding the cold crystallization of PLA. d) Storage modulus at room temperature for the nine combinations.

of PLA75PBSA25 processed at 400 rpm. Thanks to this statistical analysis, it emerged that elevated shear rate influences the elongation at break, only when is a high amount of dispersed phase is present.

Nevertheless, statistical analysis seems to show that a minimal effect of the variation in screw speed on the yielding point, above all for the blend with the lowest quantity of PBSA. To support this assumption and confirm the result, a semi-empirical model was applied: the Pukanszky model, which is valid when a material is composed of two distinct phases, whether they are two immiscible polymeric phases or a matrix with a rigid filler or fiber dispersed within it [59]. In this model B parameter is inherently structure dependent (**Equation (8)**) and it is able to correlate the yield strength of the blend with the component contributions [60].

$$ ln\left(\frac{\sigma_{blend}\left(1 + 2.5\varphi_{dispersed\ phase}\right)}{\sigma_{matrix}\left(1 - \varphi_{dispersed\ phase}\right)}\right) = B\varphi_{dispersed\ phase} \tag{8} $$

In this semi-empirical equation for the yield stress, if no special interaction exists between the components, the properties of the blends must lie between the simple additivity and zero interaction [61] (in the latter case B = 0). From Fig. 13 that even though a minimal trend is observed, there is a slight increase in compatibility with the increase in screw speed, specifically from 300 to 400 rpm.

3.6. DMTA results

As shown in Fig. 14 it can be stated regarding the elastic response of the polymer blends that the moduli decrease occur at the glass transition
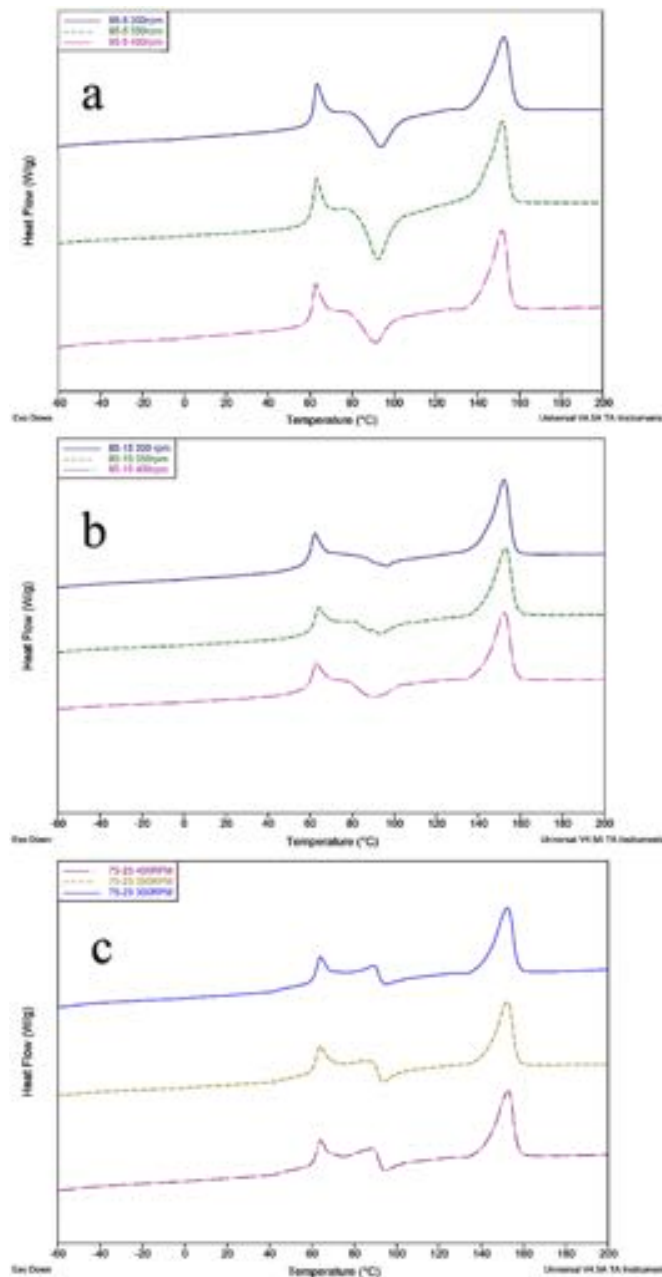
temperatures of the individual components, which are −45 °C for PBSA and 63 °C for PLA, with more or less substantial decreases depending on the amount of dispersed phase. It is noteworthy to observe a consistent trend that mirrors the results of quasi-static mechanical properties. Indeed, with a very low PBSA content (5 %), the varying shear rate does not significantly influence the properties, and when focusing on the storage modulus at room temperature, no appreciable differences are found. However, as the dispersed phase content increases, the stiffness decreases at the same temperature.

The substantial differences also persist in dynamic testing, where, for above all for PLA85PBSA15 and PLA75PBSA25 blends, the values of the elastic modulus, at room temperature, show substantial differences when switching from 300 to 400 rpm. This confirms the effect of shear rate on the stiffness/ductility ratio of the blend in the presence of a significant amount of dispersed phase (otherwise, once again, this effect is negligible).

Since, at 400 rpm a more effective dispersive and distributive mixing occurs, this results in a material with a dispersed phase characterized by smaller dimensions. Moreover, compared to the same material processed at a lower screw speed, it is possible to enhance the ductility of the matrix with a lower elastic modulus.

It can be observed, around 90 °C, an increment of the storage modulus that it is ascribed to the PLA cold crystallization, as also confirmed in the literature [62,63]; this occurs under all process conditions and this peak is more marked in formulations where the PLA amount is higher.

3.7. DSC results

To prove that the mechanical results are only influenced by the morphology induced by the process paramters, thermal analysis was carried out to exclude any effect of the crystyallinity degree. For this purpose the thermal investigation has been conducted on the filaments without removing the thermal history. The resulting thermograms are showed in Fig. 15 and main thermal properties are illustrated in Table 5.

As far as concern the thermal proeprties of PLA, it can be observed that the glass transition temperature of PLA remains almost unchanged (at around 60 °C) and it is not effected by the PBSA conent and the screw speed. A marked enthalpic relaxation peak in correspondence of the PLA T_g is also observable due to the aging PLA effect [64]. An increment of the PLA crystallinity with the PBSA content is observed; this effect is due to the nucleating effect of the dispersed PBSA phase as confirmed in a recent study [65]; an evident threshold between 5 and 10 wt%. of PBSA passing from about 13 wt% of crystallinity to 24–25 wt% was observed. It can be noticed that the crytsallinity degree is only affcetd by the PBSA content and not by the screw speed that remains almost unchanged for ech blend passing from 300 up to 400 rpm. Consequenlty, the structural characteristics shaped by the interplay of processing parameters, rather than changes in crystalline structure induced by variations in screw speed, are the primary drivers of the observed macroscopic property modifications.

As far as concern PBSA, its melting peak occurring at around 85 °C is not clear distinguishable because it is partilly overlapped by the PLA coldy crystallization peak and by the Tg PLA peak due to the aging [18]. Consequently, it was not possible to lake an accurate measurement of PBSA melting enthalpy.

4. Conclusions

In conclusion, the present work sheds light on the relationship between twin-screw extrusion parameters and morphology of biopolymeric blends based on PBSA dispersed in a PLA matrix; indeed, in order to ensure that biopolymeric blends also exhibit improved properties, it is essential to work on process parameters. Before conducting the experimental tests, a design of experiment was carried out using twin-screw extrusion simulation software. This allowed to narrow down

Fig. 15. First heating DSC Thermograms for a)PLA95PBSA5 b)PLA85PBSA15 c)PLA75PBSA25.

Table 5
DSC thermal properties for PLA-PBSA blends varying screw speeds.

Formulation name	PLA					
	ΔHm^0	ΔHm	ΔHcc	Xcc	Tm	Tcc
PLA75PBSA25 300 rpm	93	20.52	2.87	0.25	152.58	95.42
PLA75PBSA25 350 rpm	93	20.29	2.83	0.25	152.39	94.27
PLA75PBSA25 400 rpm	93	20.64	2.58	0.26	153.01	95.60
PLA85PBSA15 300 rpm	93	23.43	4.46	0.24	152.12	94.82
PLA85PBSA15 350 rpm	93	23.16	4.08	0.24	152.80	94.06
PLA85PBSA15 400 rpm	93	23.01	4.21	0.24	152.38	93.66
PLA95PBSA5 300 rpm	93	25.76	13.44	0.14	152.94	93.77
PLA95PBSA5 350 rpm	93	30.54	19.03	0.13	152.00	93.12
PLA95PBSA5 400 rpm	93	24.94	12.75	0.14	151.96	92.00

the range of influential process parameters and gain insight into how temperature, viscosity, residence time, and shear rate are affected along the screw profile by flow rate and screw speed. Definitely shear rate variation affects mechanical and rheological properties, with implications for enhancing material performance, but these effects are more evident when the dispersed phase is in major quantity in a manner way there is the possibility to act better on the mixing and size dimension of the dispersed phase.

Author contributions

Vito Gigante: Conceptualization, Methodology, Investigation, Data Curation, Validation and Writing Original Draft.

Laura Aliotta: Methodology, Data Curation, Investigation, Validation and Writing Original Draft.

Bianca Dal Pont: Methodology, Investigation, Data Curation and Review and Editing.

Vincenzo Titone: Investigation, Data Curation and Review and Editing.

Luigi Botta: Investigation, Visualization, Supervision, Review and Editing.

Francesco Paolo La Mantia: Visualization, Supervision, Resources, Writing-Review and Editing.

Andrea Lazzeri: Visualization, Supervision, Resources, Writing-Review and Editing.

Declaration of competing interest

The authors declare that they have no known competing financial interests or personal relationships that could have appeared to influence the work reported in this paper.

Data availability

Data will be made available on request.

APPENDIX A

	300 rpm 15 kg/h		
	PLA95 PBSA5	PLA85 PBSA15	PLA75 PBSA25
Avg. Residence Time (s)	34.62	34.64	34.65
T max (°C)	187.96	189.15	190.75
<Shear rate> (s^{-1})	97.77	97.77	97.77
<Viscosity> (Pa*s)	28.45	39.23	50.00
	300 rpm 20 kg/h		
	PLA95 PBSA5	PLA85 PBSA15	PLA75 PBSA25
Avg. Residence Time (s)	29.06	29.13	29.16
T max (°C)	187.54	188.74	189.93
<Shear rate> (s^{-1})	98.31	98.30	98.30
<Viscosity> (Pa*s)	28.66	39.39	50.27
	300 rpm 25 kg/h		
	PLA95 PBSA5	PLA85 PBSA15	PLA75 PBSA25
Avg. Residence Time (s)	26.02	26.08	26.11
T max (°C)	187.19	188.26	189.34
<Shear rate> (s^{-1})	101.65	101.65	101.64
<Viscosity> (Pa*s)	29.44	40.49	51.54
	350 rpm 15 kg/h		
	PLA95 PBSA5	PLA85 PBSA15	PLA75 PBSA25
Avg. Residence Time (s)	33.11	33.12	33.13
T max (°C)	188.50	190.26	192.22
<Shear rate> (s^{-1})	113.07	113.07	113.07
<Viscosity> (Pa*s)	25.62	35.46	45.29
	350 rpm 20 kg/h		
	PLA95 PBSA5	PLA85 PBSA15	PLA75 PBSA25
Avg. Residence Time (s)	27.33	27.37	27.39
T max (°C)	188.03	189.43	191.21
<Shear rate> (s^{-1})	113.59	113.59	113.59
<Viscosity> (Pa*s)	25.81	35.71	45.61
	350 rpm 25 kg/h		
	PLA95 PBSA5	PLA85 PBSA15	PLA75 PBSA25
Avg. Residence Time (s)	24.11	24.14	24.16
T max (°C)	187.56	188.84	191.19
<Shear rate> (s^{-1})	114.14	114.12	114.12
<Viscosity> (Pa*s)	26.00	35.96	45.92
	400 rpm 15 kg/h		
	PLA95 PBSA5	PLA85 PBSA15	PLA75 PBSA25
Avg. Residence Time (s)	31.96	31.98	31.98
T max (°C)	189.05	191.39	193.70
<Shear rate> (s^{-1})	128.37	128.36	128.36

(*continued*)

	400 rpm 15 kg/h		
	PLA95 PBSA5	PLA85 PBSA15	PLA75 PBSA25
<Viscosity> (Pa*s)	23.48	32.52	41.16
	400 rpm 20 kg/h		
	PLA95 PBSA5	PLA85 PBSA15	PLA75 PBSA25
Avg. Residence Time (s)	26.15	26.16	26.16
T max (°C)	188.40	190.26	192.41
<Shear rate> (s^{-1})	128.88	128.88	128.88
<Viscosity> (Pa*s)	23.70	32.83	41.95
	400 rpm 25 kg/h		
	PLA95 PBSA5	PLA85 PBSA15	PLA75 PBSA25
Avg. Residence Time (s)	22.79	22.81	22.84
T max (°C)	187.93	189.42	191.44
<Shear rate> (s^{-1})	129.41	129.41	129.41
<Viscosity> (Pa*s)	23.84	33.09	42.18

References

[1] J.P. da Costa, C. Mouneyrac, M. Costa, A.C. Duarte, T. Rocha-Santos, The role of legislation, regulatory initiatives and guidelines on the control of plastic pollution, Front. Environ. Sci. 8 (2020), https://doi.org/10.3389/fenvs.2020.00104.

[2] S. Shaikh, M. Yaqoob, P. Aggarwal, An overview of biodegradable packaging in food industry, Curr. Res. Food Sci. 4 (2021) 503–520, https://doi.org/10.1016/j.crfs.2021.07.005.

[3] A. Okunola A, O. Kehinde I, A. Oluwaseun, A. Olufiropo E, Public and environmental health effects of plastic wastes disposal: a review, Journal of Toxicology and Risk Assessment 5 (2019), https://doi.org/10.23937/2572-4061.1510021.

[4] MdG. Kibria, N.I. Masuk, R. Safayet, H.Q. Nguyen, M. Mourshed, Plastic waste: challenges and opportunities to mitigate pollution and effective management, Int. J. Environ. Res. 17 (2023) 20, https://doi.org/10.1007/s41742-023-00507-z.

[5] R. Kumar, A. Verma, A. Shome, R. Sinha, S. Sinha, P.K. Jha, R. Kumar, P. Kumar, Shubham, S. Das, P. Sharma, P.V. Vara Prasad, Impacts of plastic pollution on ecosystem services, sustainable development goals, and need to focus on circular economy and policy interventions, Sustainability 13 (2021) 9963, https://doi.org/10.3390/su13179963.

[6] N.M. Stark, L.M. Matuana, Trends in sustainable biobased packaging materials: a mini review, Materials Today Sustainability 15 (2021), 100084, https://doi.org/10.1016/j.mtsust.2021.100084.

[7] T.D. Moshood, G. Nawanir, F. Mahmud, F. Mohamad, M.H. Ahmad, A. AbdulGhani, Biodegradable plastic applications towards sustainability: a recent innovations in the green product, Clean Eng Technol 6 (2022), 100404, https://doi.org/10.1016/j.clet.2022.100404.

[8] M. Shen, B. Song, G. Zeng, Y. Zhang, W. Huang, X. Wen, W. Tang, Are biodegradable plastics a promising solution to solve the global plastic pollution? Environ. Pollut. 263 (2020), 114469 https://doi.org/10.1016/j.envpol.2020.114469.

[9] A. Costa, T. Encarnação, R. Tavares, T. Todo Bom, A. Mateus, Bioplastics: innovation for green transition, Polymers 15 (2023) 517, https://doi.org/10.3390/polym15030517.

[10] M. Bragaglia, M. Mariani, C. Sergi, F. Sarasini, J. Tirillò, F. Nanni, Polylactic acid as biobased binder for the production of 3D printing filaments for Ti6Al4V alloy manufacturing via bound metal deposition, J. Mater. Res. Technol. 27 (2023) 168–181, https://doi.org/10.1016/j.jmrt.2023.09.227.

[11] E. Balla, V. Daniilidis, G. Karlioti, T. Kalamas, M. Stefanidou, N.D. Bikiaris, A. Vlachopoulos, I. Koumentakou, D.N. Bikiaris, Poly(lactic acid): a versatile biobased polymer for the future with multifunctional properties—from monomer synthesis, polymerization techniques and molecular weight increase to PLA applications, Polymers 13 (2021) 1822, https://doi.org/10.3390/polym13111822.

[12] N. Tripathi, M. Misra, A.K. Mohanty, Durable polylactic acid (PLA)-Based sustainable engineered blends and biocomposites: recent developments, challenges, and opportunities, ACS Engineering Au 1 (2021) 7–38, https://doi.org/10.1021/acsengineeringau.1c00011.

[13] J. Urquijo, G. Guerrica-Echevarría, J.I. Eguiazábal, Melt processed PLA/PCL blends: effect of processing method on phase structure, morphology, and mechanical properties, J. Appl. Polym. Sci. 132 (2015) 1–9, https://doi.org/10.1002/app.42641.

[14] S. Su, R. Kopitzky, S. Tolga, S. Kabasci, Polylactide (PLA) and its blends with poly (butylene succinate) (PBS): a brief review, Polymers 11 (2019) 1193, https://doi.org/10.3390/polym11071193.

[15] V. Gigante, I. Canesi, P. Cinelli, M.B. Coltelli, A. Lazzeri, Rubber toughening of polylactic acid (PLA) with poly(butylene adipate-co-terephthalate) (PBAT): mechanical properties, fracture mechanics and analysis of ductile-to-brittle behavior while varying temperature and test speed, Eur. Polym. J. 115 (2019) 125–137, https://doi.org/10.1016/j.eurpolymj.2019.03.015.

[16] M.P. Arrieta, M.D. Samper, M. Aldas, J. López, On the use of PLA-PHB blends for sustainable food packaging applications, Materials 10 (2017) 1–26, https://doi.org/10.3390/ma10091008.

[17] M. Nofar, D. Sacligil, P.J. Carreau, M.R. Kamal, M.-C. Heuzey, Poly (lactic acid) blends: processing, properties and applications, Int. J. Biol. Macromol. 125 (2019) 307–360, https://doi.org/10.1016/j.ijbiomac.2018.12.002.

[18] L. Aliotta, A. Vannozzi, I. Canesi, P. Cinelli, M.B. Coltelli, A. Lazzeri, Poly(Lactic acid) (PLA)/poly(butylene succinate-co-adipate) (PBSA) compatibilized binary biobased blends: melt fluidity, morphological, thermo-mechanical and micromechanical analysis, Polymers 13 (2021) 1–22, https://doi.org/10.3390/polym13020218.

[19] P. Suwanamornlert, N. Kerddonfag, A. Sane, W. Chinsirikul, W. Zhou, V. Chonhenchob, Poly(lactic acid)/poly(butylene-succinate-co-adipate) (PLA/PBSA) blend films containing thymol as alternative to synthetic preservatives for active packaging of bread, Food Packag. Shelf Life 25 (2020), 100515, https://doi.org/10.1016/j.fpsl.2020.100515.

[20] A. Gaspar-Cunha, P. Costa, A. Delbem, F. Monaco, M.J. Ferreira, J. Covas, Evolutionary multi-objective optimization of extrusion barrier screws: data mining and decision making, Polymers 15 (2023), https://doi.org/10.3390/polym15092212.

[21] M.A. Emin, H.P. Schuchmann, A mechanistic approach to analyze extrusion processing of biopolymers by numerical, rheological, and optical methods, Trends Food Sci. Technol. 60 (2017) 88–95, https://doi.org/10.1016/j.tifs.2016.10.003.

[22] M. Decol, W.M. Pachekoski, E.H. Segundo, L.A. Pinheiro, D. Becker, Effects of processing conditions on hybrid filler selective localization, rheological, and thermal properties of poly(ε-caprolactone)/poly(lactic acid) blends, J. Appl. Polym. Sci. 137 (2020), 48711, https://doi.org/10.1002/app.48711.

[23] M. Hyvärinen, R. Jabeen, T. Kärki, The modelling of extrusion processes for polymers—a review, Polymers 12 (2020) 1306, https://doi.org/10.3390/polym12061306.

[24] M.J. Stevens, J.A. Covas, Extruder Principles and Operation, Springer Science & Business Media, 2012.

[25] A. D'Anna, R. Arrigo, A. Frache, Rheology, morphology and thermal properties of a PLA/PHB/clay blend nanocomposite: the influence of process parameters, J. Polym. Environ. 30 (2022) 102–113, https://doi.org/10.1007/s10924-021-02186-3.

[26] F.P. La Mantia, M. Morreale, L. Botta, M.C. Mistretta, M. Ceraulo, R. Scaffaro, Degradation of polymer blends: a brief review, Polym. Degrad. Stabil. 145 (2017) 79–92, https://doi.org/10.1016/j.polymdegradstab.2017.07.011.

[27] R. Cardinaels, P. Moldenaers, Morphology development in immiscible polymer blends, in: Polymer Morphology, John Wiley & Sons, Inc, Hoboken, NJ, USA, 2016, pp. 348–373, https://doi.org/10.1002/9781118892756.ch19.

[28] B. Vergnes, Influence of processing conditions on the preparation of clay-based nanocomposites by twin-screw extrusion, Int. Polym. Process. 34 (2019) 482–501, https://doi.org/10.3139/217.3827.

[29] B. Vergnes, Average shear rates in the screw elements of a corotating twin-screw extruder, Polymers 13 (2021) 304, https://doi.org/10.3390/polym13020304.

[30] O.S. Carneiro, J.A. Covas, B. Vergnes, Experimental and theoretical study of twin-screw extrusion of polypropylene, J. Appl. Polym. Sci. 78 (2000) 1419–1430, https://doi.org/10.1002/1097-4628(20001114)78:7<1419::AID-APP130>3.0.CO;2-B.

[31] A. Durin, P. De Micheli, H.-C. Nguyen, C. David, R. Valette, B. Vergnes, Comparison between 1D and 3D approaches for twin-screw extrusion simulation, Int. Polym. Process. 29 (2014) 641–648, https://doi.org/10.3139/217.2951.

[32] V. Gigante, L. Aliotta, I. Canesi, M. Sandroni, A. Lazzeri, M.-B. Coltelli, P. Cinelli, Improvement of interfacial adhesion and thermomechanical properties of PLA based composites with wheat/rice bran, Polymers 14 (2022) 3389, https://doi.org/10.3390/polym14163389.

[33] Q. Jiang, J.L. White, J. Yang, A global model for closely intermeshing counter-rotating twin screw extruders with flood feeding, Int. Polym. Process. 25 (2010) 223–235, https://doi.org/10.3139/217.2333.

[34] S. Rodrigues, S. Miri, R.G. Cole, A.A. Postigo, M.A. Saleh, A. Dondish, G. W. Melenka, K. Fayazbakhsh, Towards optimization of polymer filament tensile test for material extrusion additive manufacturing process, J. Mater. Res. Technol. 24 (2023) 8458–8472, https://doi.org/10.1016/j.jmrt.2023.05.088.

[35] E.W. Fischer, H.J. Sterzel, G. Wegner, Investigation of the structure of solution grown crystals of lactide copolymers by means of chemical reactions, Kolloid-Z. Z. Polym. 251 (1973) 980–990, https://doi.org/10.1007/BF01498927.

[36] K. Wilczyński, K. Buziak, A. Lewandowski, A. Nastaj, K.J. Wilczyński, Rheological basics for modeling of extrusion process of wood polymer composites, Polymers 13 (2021) 622, https://doi.org/10.3390/polym13040622.

[37] A. Poulesquen, B. Vergnes, A study of residence time distribution in co-rotating twin-screw extruders. Part I: theoretical modeling, Polym. Eng. Sci. 43 (2003) 1841–1848, https://doi.org/10.1002/pen.10156.

[38] F. Bernardo, J.A. Covas, S. V Canevarolo, On-line optical monitoring of the mixing performance in Co-rotating twin-screw extruders, Polymers 14 (2022) 1152, https://doi.org/10.3390/polym14061152.

[39] M. Salzano de Luna, G. Filippone, Effects of nanoparticles on the morphology of immiscible polymer blends – challenges and opportunities, Eur. Polym. J. 79 (2016) 198–218, https://doi.org/10.1016/j.eurpolymj.2016.02.023.

[40] P. Van Puyvelde, S. Velankar, P. Moldenaers, Rheology and morphology of compatibilized polymer blends, Curr. Opin. Colloid Interface Sci. 6 (2001) 457–463, https://doi.org/10.1016/S1359-0294(01)00113-3.

[41] J. Zhang, Y. Han, Z. Wang, Accelerating effects of flow behavior index n on breakup dynamics for droplet evolution in non-Newtonian fluids, Materials 15 (2022) 4392, https://doi.org/10.3390/ma15134392.

[42] L.A. Utracki, Z.H. Shi, Development of polymer blend morphology during compounding in a twin-screw extruder. Part I: droplet dispersion and coalescence? a review, Polym. Eng. Sci. 32 (1992) 1824–1833, https://doi.org/10.1002/pen.760322405.

[43] J.K. Lee, C.D. Han, Evolution of polymer blend morphology during compounding in a twin-screw extruder, Polymer (Guildf) 41 (2000) 1799–1815, https://doi.org/10.1016/S0032-3861(99)00325-0.

[44] P. Pötschke, D.R. Paul, Formation of Co-continuous structures in melt-mixed immiscible polymer blends, J. Macromol. Sci. Polym. Rev. 43 (2003) 87–141, https://doi.org/10.1081/MC-120018022.

[45] L. Delamare, B. Vergnes, Computation of the morphological changes of a polymer blend along a twin-screw extruder, Polym. Eng. Sci. 36 (1996) 1685–1693, https://doi.org/10.1002/pen.10565.

[46] M.A. Huneault, Z.H. Shi, L.A. Utracki, Development of polymer blend morphology during compounding in a twin-screw extruder. Part IV: a new computational model with coalescence, Polym. Eng. Sci. 35 (1995) 115–127, https://doi.org/10.1002/pen.760350114.

[47] A. Basolo, PLA/PHBH Compounding by Twin-Screw Extrusion : Simulation-Based Evaluation of the Processing Parameters, Politecnico di Torino, 2021.

[48] C.B. Bucknall, D.S. Ayre, D.J. Dijkstra, Detection of rubber particle cavitation in toughened plastics using thermal contraction tests, Polymer (Guildf) 41 (2000) 5937–5947.

[49] A. Lazzeri, C.B. Bucknall, Applications of a dilatational yielding model to rubber-toughened polymers, Polymer (Guildf) 36 (1995) 2895–2902, https://doi.org/10.1016/0032-3861(95)94338-T.

[50] V. Gigante, L. Aliotta, M.B. Coltelli, P. Cinelli, L. Botta, F.P. La Mantia, A. Lazzeri, Fracture behavior and mechanical, thermal, and rheological properties of biodegradable films extruded by flat die and calendar, J. Polym. Sci. 58 (2020) 3264–3282, https://doi.org/10.1002/pol.20200555.

[51] M. Nofar, A. Maani, H. Sojoudi, M.C. Heuzey, P.J. Carreau, Interfacial and rheological properties of PLA/PBAT and PLA/PBSA blends and their morphological stability under shear flow, J Rheol (N Y N Y). 59 (2015) 317–333, https://doi.org/10.1122/1.4905714.

[52] W. Abdallah, A. Mirzadeh, V. Tan, M. Kamal, Influence of nanoparticle pretreatment on the thermal, rheological and mechanical properties of PLA-PBSA nanocomposites incorporating cellulose nanocrystals or montmorillonite, Nanomaterials 9 (2018) 29, https://doi.org/10.3390/nano9010029.

[53] A. Anstey, A. Codou, M. Misra, A.K. Mohanty, Novel compatibilized nylon-based ternary blends with polypropylene and poly(lactic acid): fractionated crystallization phenomena and mechanical performance, ACS Omega 3 (2018) 2845–2854, https://doi.org/10.1021/acsomega.7b01569.

[54] W. Hale, J.H. Lee, H. Keskkula, D.R. Paul, Effect of PBT melt viscosity on the morphology and mechanical properties of compatibilized and uncompatibilized blends with ABS, Polymer (Guildf) 40 (1999) 3621–3629, https://doi.org/10.1016/S0032-3861(98)00583-7.

[55] Y. Ding, C. Abeykoon, Y.S. Perera, The effects of extrusion parameters and blend composition on the mechanical, rheological and thermal properties of LDPE/PS/PMMA ternary polymer blends, Advances in Industrial and Manufacturing Engineering 4 (2022), 100067, https://doi.org/10.1016/j.aime.2021.100067.

[56] L. Aliotta, A. Vannozzi, P. Cinelli, M.-B. Coltelli, A. Lazzeri, Essential work of fracture and evaluation of the interfacial adhesion of plasticized PLA/PBSA blends with the addition of wheat bran by-product, Polymers 14 (2022) 615, https://doi.org/10.3390/polym14030615.

[57] L. Aliotta, V. Gigante, B. Dal Pont, F. Miketa, M.-B. Coltelli, A. Lazzeri, Tearing fracture of poly(lactic acid) (PLA)/poly(butylene succinate-co-adipate) (PBSA) cast extruded films: effect of the PBSA content, Eng. Fract. Mech. 289 (2023), 109450, https://doi.org/10.1016/j.engfracmech.2023.109450.

[58] D. Lascano, L. Quiles-Carrillo, R. Balart, T. Boronat, N. Montanes, Toughened poly (lactic acid)-PLA formulations by binary blends with poly(butylene succinate-co-adipate)-PBSA and their shape memory behaviour, Materials 12 (2019), https://doi.org/10.3390/ma12040622.

[59] B. Pukánszky, F. Tüdős, Miscibility and mechanical properties of polymer blends, Makromol. Chem. Macromol. Symp. 38 (1990) 221–231, https://doi.org/10.1002/masy.19900380118.

[60] B. Imre, B. Pukánszky, Compatibilization in bio-based and biodegradable polymer blends, Eur. Polym. J. 49 (2013) 1215–1233, https://doi.org/10.1016/j.eurpolymj.2013.01.019.

[61] B. Bozsódi, V. Romhányi, P. Pataki, D. Kun, K. Renner, B. Pukánszky, Modification of interactions in polypropylene/lignosulfonate blends, Mater. Des. 103 (2016) 32–39, https://doi.org/10.1016/j.matdes.2016.04.061.

[62] M. Cristea, D. Ionita, M.M. Iftime, Dynamic mechanical analysis investigations of pla-based renewable materials: how are they useful? Materials 13 (2020) 1–24, https://doi.org/10.3390/ma13225302.

[63] M.E. Mngomezulu, A.S. Luyt, M.J. John, Morphology, thermal and dynamic mechanical properties of poly(lactic acid)/expandable graphite (PLA/EG) flame retardant composites, J. Thermoplast. Compos. Mater. 32 (2019) 89–107, https://doi.org/10.1177/0892705717744830.

[64] J. Ostrowska, W. Sadurski, M. Paluch, P. Tyński, J. Bogusz, The effect of poly (butylene succinate) content on the structure and thermal and mechanical properties of its blends with polylactide, Polym. Int. 68 (2019) 1271–1279, https://doi.org/10.1002/pi.5814.

[65] M.B. Coltelli, L. Aliotta, G. Fasano, F. Miketa, F. Brkić, R. Alonso, M. Romei, P. Cinelli, I. Canesi, V. Gigante, A. Lazzeri, Recyclability studies on poly(lactic acid)/Poly(butylene succinate-co-adipate) (PBSA) biobased and biodegradable films, Macromol. Mater. Eng. (2023), https://doi.org/10.1002/mame.202300136.